

Optimization, Electromagnetic Analysis, and Thermal Evaluation of a New FSPM Generator with Efficient Employment of Neodymium Magnets Sandwiched Between Rotor Segments

Amir Ebrahimi Shohani¹, Mohammad Farahzadi², Sohrab Abbasian³,
 Aghil Ghaheri⁴, Karim Abbaszadeh¹, Salman Ali⁵

Abstract – Flux-Switching Permanent Magnet (FSPM) machines have gained significant popularity in various applications due to their excellent high-power density. This paper introduces a new outer-rotor FSPM generator designed for wind turbine applications. The widths of the magnets, rotor tooth angles, and stator tooth angles are selected as design variables and optimized using the Taguchi method and the 3-D finite element method to enhance the generator's performance. The optimization results demonstrate considerable improvements in no-load phase voltage, total harmonic distortion, and cogging torque. Additionally, the thermal performance evaluation indicates that the temperature of the stator core is nearly twice that of the rotor core. This finding supports the decision to place neodymium magnets in the rotor rather than in the stator core, as these magnets are susceptible to demagnetization at high temperatures. Furthermore, the results reveal that the proportion of magnets relative to the total machine volume is significantly lower compared to other FSPM generators while still maintaining a high-power density. **Copyright © 2025 The Authors.**

Published by Praise Worthy Prize S.r.l. This article is open access published under the CC BY-NC-ND license (<http://creativecommons.org/licenses/by-nc-nd/3.0/>).

Keywords: Finite Element Method, Flux-Switching Machines, Loss Density, Permanent Magnet, Taguchi Method, Temperature Distribution, Thermal Evaluation, Wind Turbines

Nomenclature

η_{Elec}	Electric system efficiency
η_{GB}	Gearbox efficiency
η_{Gen}	Generator efficiency
λ	Tip-speed ratio
ρ	Air density [kg/m ³]
φ	Power factor
ω_R	Blades' angular frequency [rad/s ⁻¹]
ω_r	Rotor's rotational speed [rad/min]
A_W	Blades' swept area [m ²]
A_w	Electrical loading [A/m]
B_g	Average no-load air-gap flux density [T]
$C_p(\lambda)$	Power coefficient
C_s	Rotor pole arc
E_m	Coil back-EMF [V]
f_1, \dots, f_5	Objective functions
f_e	Electrical frequency [Hz]
F_j	Weighted function
I_m	Coil current [A]
k_l	Leakage factor
k_{sat}	Saturation factor
k_w	Winding factor
L	Machine's length [m]
m	Number of phases
$M_{ij}(f)$	Analysis of mean
n_{ph}	Phase turn number

N_r	Rotor pole pair
N_s	Stator pole number
P_{eff}	Effective power of a wind turbine [W]
P_G	Generator output power [W]
P_{wt}	Wind turbine power [W]
R	Blades' radius [m]
R_{so}	Stator outer radius [m]
U_w	Wind speed [m/s]
V_1, V_2, V_3	Design variables
EMF	Electromotive Force
FEM	Finite Element Method
FSPM	Flux Switching Permanent Magnet
HAWT	Horizontal Axis Wind Turbines
PM	Permanent Magnet
RMS	Root Mean Square
THD	Total Harmonic Distortion
VAWT	Vertical Axis Wind Turbines

I. Introduction

Greenhouse gas emissions represent a critical challenge for societies globally, significantly contributing to both global warming and climate change [1]. The predominant source of these emissions is the conventional power plants that rely on fossil fuels to generate electricity [2]. These power plants account for almost 35% of global greenhouse

gas emissions [3]. Furthermore, price fluctuations and potential shortages of fossil fuels are other reasons for governments to explore alternatives such as renewable energy [4]. Renewable energy, also known as green energy, is generated from natural resources and can be divided into five main categories: hydro energy, wind energy, solar energy, bioenergy, and geothermal energy [5]. It is noteworthy that wind energy is the second most prevalent renewable energy source for electricity generation worldwide, following hydro energy [6]. This is primarily due to its easy maintenance, simple structure, cost-efficiency, and recent advancements in wind turbine technology [7], [8]. Furthermore, the generator is a crucial component of the wind turbine system. Hence, the type of generator should be selected carefully to meet the desired requirements. Subsequently, Flux-Switching Permanent-Magnet (FSPM) machines are well-known for their high power density, high efficiency, reliability, safety, and continuous operation [9]. These qualities make FSPM machines an excellent choice for wind turbine applications [10]. In conventional FSPM machines, the PMs and winding are installed in the stator, and the rotor benefits from a simple, solid, and sturdy structure [11]. This design makes conventional FSPM machines excellent candidates for high-speed applications [12]. However, in terms of heat management, the temperature of the stator core can be nearly twice as high as that of the rotor core [13].

Additionally, placing Permanent Magnets (PMs) in the stator core may lead to demagnetization, particularly for neodymium magnets, which are sensitive and can quickly lose their magnetic properties under high-temperature conditions [14]. To address this challenge, this paper presents a new outer-rotor FSPM generator that utilizes a simplified stator core while the neodymium magnets are sandwiched between rotor segments. In [15], [16], conventional FSPM machines were analyzed. Both machines employed neodymium magnets in the stator core without considering the risk of demagnetization under high-temperature conditions, and they featured an inner rotor configuration. Moreover, the studies did not investigate the optimization processes related to these machines. A novel inner-rotor FSPM machine featuring E-shaped stator teeth and magnets located within the teeth was introduced in [17]. While this configuration is innovative, it utilizes a relatively high volume of neodymium magnets. The proportion of magnet volume to the overall machine volume is approximately 8%, indicating that the manufacturing cost is considerable.

Additionally, a new modular-stator outer-rotor FSPM machine was presented in [18]. However, this study did not address the thermal behavior of the proposed machine or the risk of magnet demagnetization, focusing solely on its electromagnetic performance. In [19], an outer-rotor hybrid-excited FSPM generator was introduced. To address the potential issue of demagnetization in neodymium magnets, these magnets were placed in the rotor, while ferrite magnets, less prone to demagnetization at high temperatures, were positioned in the stator core.

Additionally, the stator core was enhanced with several

flux barriers. Although the power density of the generator discussed in [19] is slightly higher than that of the proposed generator in this paper, the use of ferrite magnets and flux barriers complicates the manufacturing of the stator core, ultimately raising the overall production cost.

In recent studies, as presented in [20] and [21], two distinctive configurations of outer rotor flux-switching permanent magnet machines have been examined. The study in [20] describes a segmented rotor core with neodymium permanent magnets affixed to the stator teeth.

Conversely, [21] explores a design where the neodymium PMs are positioned in a sandwiched arrangement on the stator teeth. In contrast, [22] and [23] focus on two different configurations of inner rotor FSPM machines. The work in [22] indicates that the stator core is also segmented but places the neodymium PMs internally within the stator teeth. Meanwhile, in the design presented in [23], the neodymium PMs are situated between the stator teeth, highlighting a different approach to magnet placement within the machine structure.

Moreover, additional insights into the inner rotor FSPM machines can be found in [24]. These studies elaborate on designs incorporating neodymium PMs arranged in radial and circumferential orientations within the stator core, thereby addressing various geometric considerations that may impact operational efficiency and performance.

However, one significant challenge associated with conventional FSPM machines, whether the outer rotor, as discussed in [20] and [21] or inner rotor configurations highlighted in [22] through [24], is the potential for demagnetization of the permanent magnets. This issue arises primarily because the PMs are typically situated within the stator core, which tends to experience higher temperatures than the rotor core. Neodymium PMs are particularly susceptible to thermal degradation; exposure to elevated temperatures can lead to a substantial loss of their magnetization properties, which can critically impair the performance and reliability of the machine.

Understanding and mitigating the effects of thermal exposure on PMs is thus essential in the design and operation of FSPM machines. Researchers and engineers must consider innovative materials, cooling strategies, and design modifications that can preserve magnetic integrity under operational conditions, ultimately improving the durability and efficiency of these advanced machines. A comprehensive thermal modeling approach for a flux-switching permanent magnet machine was developed in [25], emphasizing key factors such as anisotropic thermal conductivity, thermal contact resistance, and convection heat transfer in the air gap, which are crucial for accurate thermal analysis. Cheng et al. [26] presented empirical data regarding the losses and temperature behavior of a nine-phase FSPM machine under nominal loading conditions, providing insights into its thermal performance. Moreover, [27] introduces a hybrid analytical thermal model that integrates the Lumped Parameter Modeling (LPM) and analytical methods, effectively estimating the temperature distribution of the permanent magnets in surface-mounted permanent

magnet synchronous machines. [28] elaborates on a thermal transient analysis encompassing all components of a single-sided axial flux permanent magnet machine, employing LPM to assess temperature variations during operational conditions. Meanwhile, Glowacz has explored innovative fault diagnosis methodologies based on thermal imaging analysis. His work includes a thermal fault diagnosis method tailored for angle grinders, as well as a thermographic evaluation approach for identifying ventilation faults in brushless direct current motors [29], [30], [31]. In another significant contribution, the authors in [32] focus on the thermal characteristics of a transverse flux permanent magnet generator that utilizes Halbach-array permanent magnets, presenting a detailed thermodynamic analysis. Furthermore, [33] offers an in-depth 3-D thermal analysis employing the LPM technique specifically for a rotor-excited axial field FSPM machine, highlighting the intricacies involved in the thermal management of these advanced electromagnetic systems.

These studies collectively enhance the understanding of thermal dynamics in various types of permanent magnet machines, revealing critical insights into their operational efficiency, reliability, and the implications of thermal behaviors in optimizing machine performance and fault diagnosis. Despite the growing research on FSPM machines, many designs prioritize performance under ideal conditions rather than accounting for real-world operational constraints such as fluctuating temperatures, environmental exposure, or long-term material degradation. Maintenance opportunities are limited in practical applications, especially in offshore or remote wind farms, and systems must endure varying thermal loads over extended periods. As such, there is a pressing need for machine architectures that perform efficiently and maintain structural and magnetic integrity with minimal maintenance. This shift in focus from pure performance metrics to durability and thermal resilience represents a crucial step in bridging the gap between laboratory designs and industrial deployment. Based on the literature review, researchers have generally overlooked the potential risk of PM demagnetization under high-temperature conditions, as well as the volume of the PM itself. This paper aims to introduce a new FSPM generator that employs neodymium magnets in the rotor core to prevent demagnetization, as the rotor core operates at a significantly lower temperature than the stator core.

Additionally, the generator features a simplified structure for the stator core, and the ratio of PM volume to the overall machine volume is less than 3%. This design choice significantly reduces manufacturing costs. The following section discusses the generator's application, key equations for initial design, and the configuration of the proposed generator. In Section III, the Taguchi method is introduced and utilized for optimization. Section IV presents the electromagnetic performance of the machine, which is classified into two groups: no-load and full-load conditions. Also, the thermal behavior of the generator is discussed in Section V. Finally, the results are summarized in Section VI.

II. Generator's Application and Structure

This section is organized into three categories. First, the wind turbine specifications will be discussed as they pertain to the generator's application. Next, the related size equations will be introduced, and finally, the generator's topology will be presented.

II.1. Wind Turbines

Wind turbines can be classified into two groups based on the axis of rotation [34]. These groups are Vertical-Axis Wind Turbines (VAWT) and Horizontal-Axis Wind Turbines (HAWT), as shown in Fig. 1. VAWTs offer various advantages over HAWTs. For instance, in HAWT, the generator and gearbox are located at the top of the tower, whereas in VAWTs, these components are located at the ground level, making them easier to maintain.

Moreover, unlike HAWT, VAWT is independent of the wind direction in generating power. Also, VAWT's maximum efficiency can reach more than 70%, while this value for HAWT is less than 60% [35]. It is important to note that the maximum theoretical efficiency for converting kinetic energy into mechanical energy is approximately 59.3%, according to the Lanchester-Betz law [36]. Hence, this study considers VAWT to be the generator's application. Furthermore, the wind turbine power can be presented as follows [19]:

$$P_{WT} = \frac{1}{2} \rho A_w U_w^3 C_p(\lambda) \quad (1)$$

where ρ , A_w , U_w and $C_p(\lambda)$ are air density (kg/m^3), blades swept area (m^2), wind speed (m/s), and power coefficient, respectively. Also, λ is the tip-speed ratio and can be calculated as below:

$$\lambda = \frac{\omega_R R}{U_w} \quad (2)$$

where ω_R and R are blades' angular frequency (rad s^{-1}) and radius (m), respectively.

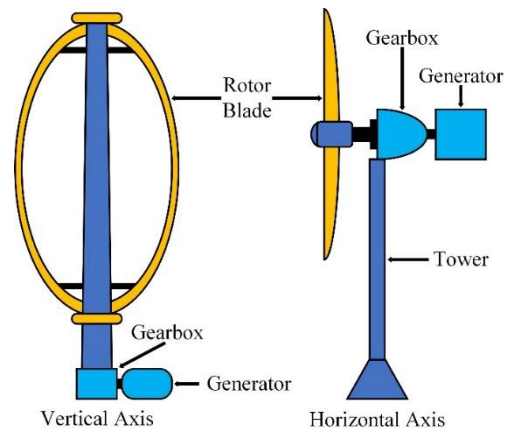


Fig. 1. Schematic of vertical-axis and horizontal-axis wind turbines

Moreover, the power coefficient equation can be described as follows [37]:

$$C_p(\lambda) = 0.73 \left(\frac{151}{\lambda} - 13.65 \right) e^{\left(\frac{-18.4}{\lambda} + 0.055 \right)} \quad (3)$$

Consequently, several factors must be considered to determine the wind turbine's effective output power. The first factor is η_{GB} , and can be defined as the gearbox efficiency. It is evident that the power losses in a gearbox are due to the tooth friction and bearings. Moreover, η_{Gen} can be expressed as the generator's efficiency. Finally, the electric power losses in the cables, control systems, and inverters can be considered in η_{Elec} [38]. Therefore, the total power conversion efficiency can be defined as follows:

$$\eta_T = \eta_{GB} \eta_{Gen} \eta_{Elec} \quad (4)$$

Hence, the effective output power of a wind turbine can be expressed as below [39]:

$$P_{eff} = \eta_T P_{WT} \quad (5)$$

II.2. Initial Design

Obtaining an accurate power-size equation is a critical phase in the design of electrical machines, as it provides the initial geometric values needed for the machine. Once these geometric values are established, they must be optimized. Although the final power-size equation is similar across different types of electrical machines, it is essential to consider factors such as leakage, winding, and saturation. These factors can vary for every electric machine; ignoring them can lead to incorrect data. Hence, this part presents the most important equations related to flux-switching machines. Electrical frequency plays an essential part in the FSPM machines and can be seen in almost all the related equations. Therefore, (6) expresses the electrical frequency equation in the FSPM machines [40]:

$$f_e = \frac{N_r \omega_r}{60} \quad (6)$$

where N_r and ω_r are the rotor pole pair and the rotor's rotational speed (rad/min), respectively. Also, the stator pole number can be calculated as follows:

$$\begin{aligned} N_s &= 2(N_r \pm j), \\ j &= 1, 2, 3, \dots \end{aligned} \quad (7)$$

Moreover, the maximum value of coil back-EMF and current should be calculated to determine the power-size equation. Hence, the peak value of the coil back-EMF can be written as follows [41]:

$$E_m = 2\pi \frac{N_r}{N_s} n_{ph} B_g R_{so} L k_l k_{sat} C_s \omega_r \quad (8)$$

where n_{ph} , B_g , R_{so} , L , k_l , k_{sat} , and C_s are phase turn number, average no-load air-gap flux density (T), stator outer radius (m), effective machine's length (m), leakage factor, saturation factor, and rotor pole arc factor, respectively.

Subsequently, the peak value of the coil current can be represented as below:

$$I_m = \sqrt{2} \frac{A_w \pi R_{so}}{k_w m n_{ph}} \quad (9)$$

where A_w , k_w , and m are the electrical loading (A/m), the winding factor, and the number of phases, respectively.

Finally, the stator outer radius can be written as below [42]:

$$R_{so} = \sqrt{\frac{30 N_s k_w P_G}{\sqrt{2} \pi^3 N_r L A_w B_g k_l k_{sat} C_s \omega_r \cos(\varphi)}} \quad (10)$$

where P_G and $\cos(\varphi)$ are the generator output power (W) and the power factor, respectively.

II.3. Configuration of the Generator

Fig. 2 illustrates the structure of the proposed generator. As can be seen, the rotating components include the housing, rotor segments, and neodymium magnets, while the stationary components consist of the stator core and the winding. Ten neodymium magnets are positioned between steel rotor segments and are magnetized counter-clockwise. Additionally, the rotor segments are attached to the aluminum housing. The three-phase winding is located in the stator core, with each phase made up of four coils, resulting in a total of twenty-four slots within the laminated steel stator core. Also, the initial design parameters of the proposed generator are listed in Table I.

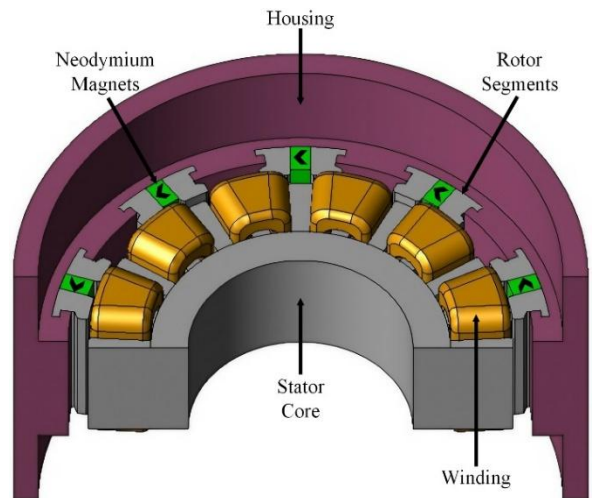


Fig. 2. The 3-D configuration of the proposed generator

TABLE I
INITIAL DESIGN PARAMETERS OF THE PROPOSED GENERATOR

Parameter	Value	Unit
Phase number	3	---
Stator slot number	24	---
Rotor pole pair number	10	---
Turns per coil	200	---
Rotor outer diameter	200.7	mm
Stator outer diameter	170	mm
Air-gap length	0.65	mm
Rotational speed	750	rpm
Residual flux density of PM	1.2	T

III. Optimization by Taguchi Method

The optimization of initial parameters is an inevitable step in the electric machine design. This section focuses on optimizing the primary parameters using the Taguchi method.

Fig. 3 depicts the process flowchart corresponding to the optimization procedure. Initially, it is essential to define the objective functions. In this context, the selected objective functions include the open-circuit phase voltage, Total Harmonic Distortion (THD) of the no-load voltage, and the cogging torque. The main goal of this optimization is to maximize the no-load voltage while minimizing the THD and the cogging torque. Choosing the design variables is another step of the optimization process.

Hence, the geometric parameters of the proposed generator have been identified as design variables. These include the width of neodymium PMs, the rotor tooth angle, and the stator tooth angle, which have been chosen as the design variables, which are denoted as V1, V2, and V3, respectively, in Table II. Furthermore, it is crucial to establish a range of values for each parameter within the Taguchi method. This range is represented as different levels. The specified levels for each parameter are detailed in Table III. Due to the presence of three parameters, each with five levels, a total of $5^3=123$ Finite Element Method (FEM) simulations should be run. This requirement significantly increases the computational time of the optimization procedure and demands a large-capacity memory system. The Taguchi method introduces orthogonal arrays to address this issue, considerably reducing the number of necessary simulations. The orthogonal arrays utilized in this study are listed in Table IV. Additionally, the average value (analysis of mean) of the objective functions at various levels of the optimization variables can be expressed as (11) [43].

$$M_{ij}(f) = \frac{1}{5}(f(1) + f(2) + f(3) + f(4) + f(5)) \quad (11)$$

where i, j , and f are one of the optimization variables V1, V2, and V3, the number of variables' levels, and the optimization's objective functions voltage, THD, and cogging torque, respectively. Consequently, Figs. 4 illustrate the analysis of the mean of the open-circuit phase voltage, THD, and the cogging torque, respectively.

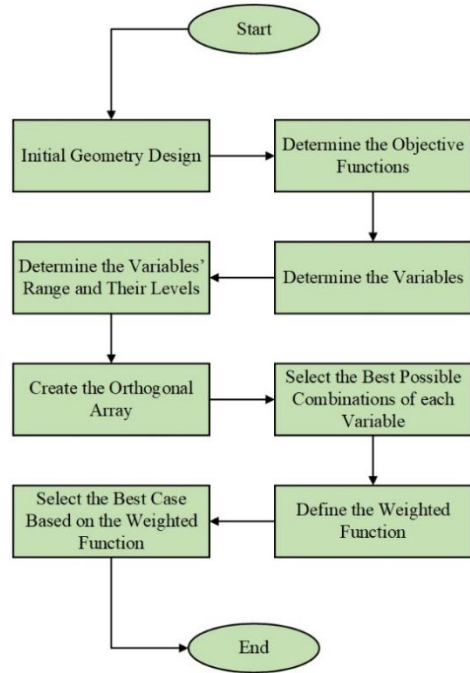


Fig. 3. Flowchart of the optimization procedure of the proposed generator

TABLE II
VARIABLES OF THE PROPOSED GENERATOR

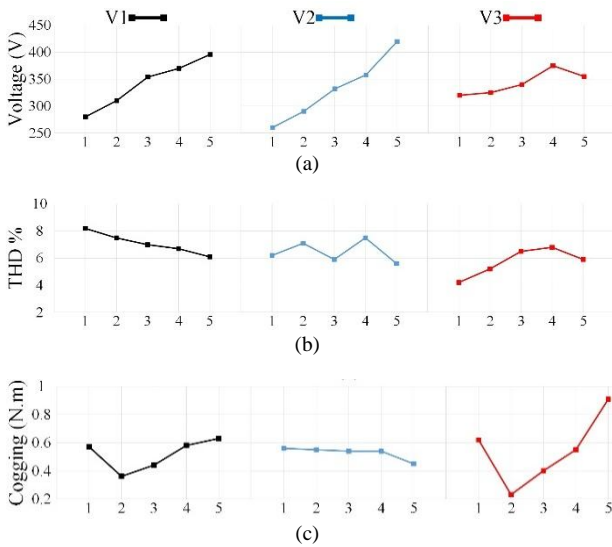
Variables	Definition	Symbol	Unit
V1	Width of neodymium PMs	α	mm
V2	Rotor tooth angle	β	deg
V3	Stator tooth angle	γ	deg

TABLE III
LEVELS OF DEFINED VARIABLES

Variables	Level 1	Level 2	Level 3	Level 4	Level 5
V1	6	6.5	7	7.5	8
V2	6.5	7.5	8.5	9.5	10.5
V3	7	7.5	8	8.5	9

TABLE IV
ORTHOGONAL ARRAY

Run	V1	V2	V3
1	1	1	1
2	1	2	2
3	1	3	3
4	1	4	4
5	1	5	5
6	2	1	2
7	2	2	3
8	2	3	4
9	2	4	5
10	2	5	1
11	3	1	3
12	3	2	4
13	3	3	5
14	3	4	1
15	3	5	2
16	4	1	4
17	4	2	5
18	4	3	1
19	4	4	2
20	4	5	3
21	5	1	5
22	5	2	1
23	5	3	2
24	5	4	3
25	5	5	4



Figs. 4. The average value of various objective functions: (a) no-load voltage; (b) THD; (c) cogging torque

Furthermore, Table V presents the most appropriate combination of each design variable, yielding the most favorable values for the objective functions.

As can be seen, the fifth level of the V2 parameter is the most optimal choice across all objective functions.

Also, the fifth level of the V1 parameter is the most favorable option for the no-load voltage and THD, while the second level leads to the lowest value of the cogging torque.

Consequently, the fourth level of the V3 parameter yields the highest no-load voltage value, whereas the first level corresponds to the minimum value of THD.

Additionally, the second level of this parameter results in the minimum value of cogging torque. Since the first and second levels of the V3 have an extreme impact on the THD and cogging torque, they are preferred over the fourth level. It is evident that there is a contrast and conflict in selecting the best combinations of design variables. Table VI represents the most optimal combinations. Finding the optimal case is challenging and often confusing. Thus, to tackle this issue, the weighted function approach is employed to transform the multi-objective optimization into a single-optimization problem [44]. The weighted function can be expressed as follows:

$$F_j = \frac{THD_j \times Cogging_j}{Voltage_j} \times 100 \quad (12)$$

where j represents the case number. Clearly, the lowest value of F_j presents the most optimum case. Table VII depicts the weighted-function value for each case.

TABLE V
OPTIMAL COMBINATIONS OF DESIGN VARIABLES FOR EACH OBJECTIVE FUNCTION

Objective Functions	V1	V2	V3
Open-circuit phase voltage	5	5	4
THD	5	5	1
Cogging torque	2	5	2

TABLE VI
OPTIMUM COMBINATIONS OF DESIGN VARIABLES

Case	V1	V2	V3	Voltage (V)	THD%	Cogging (N m)
1	5	5	1	398.4	6.4	0.34
2	5	5	2	397.1	10.11	0.31
3	2	5	1	380	7	0.32
4	2	5	2	384	7.4	0.31

TABLE VII
THE WEIGHTED FUNCTION VALUE

Case	F_j
1	0.546
2	0.788
3	0.589
4	0.597

According to the findings presented in Table VII, case 1 presents the most optimal configuration. Therefore, the width of the neodymium magnets should be set at 8 mm.

Additionally, the rotor tooth angle should be configured at 10.5 degrees, while the stator tooth angle should be adjusted to 7 degrees. Moreover, the values of the objective functions before and after optimization are listed in Table VIII. It can be seen that the no-load voltage value increased by 26.37%, while the THD and cogging torque decreased by 42.85% and 65.3%, respectively.

IV. Electromagnetic Analysis

The electromagnetic performance of the proposed generator must be evaluated to assess the accuracy of the optimization process. This section outlines the generator's specifications under both no-load and full-load conditions.

The first part emphasizes the no-load specifications, presenting the no-load voltage and its harmonics, the air-gap flux density, and the cogging torque. The second part addresses full-load specifications, detailing the magnetic flux distributions in various components of the generator, the loss density, and the output torque.

IV.1. No-Load Characteristics

The no-load condition, wherein the stator winding is electrically disconnected, provides valuable insight into the intrinsic behavior of the generator when solely excited by the embedded permanent magnets. This test condition not only validates the magnetic design but also reveals potential issues, such as harmonic distortion and cogging torque, that could affect performance in real-world applications. Fig. 5(a) illustrates the open-circuit phase voltage waveform, yielding a Root Mean Square (RMS) value of 281.71 V. This relatively high output voltage under no-load conditions confirms the efficacy of the magnetic circuit and the adequacy of flux linkage between the rotor-mounted permanent magnets and the stator core.

TABLE VIII
A COMPARISON OF VALUES BEFORE AND AFTER OPTIMIZATION

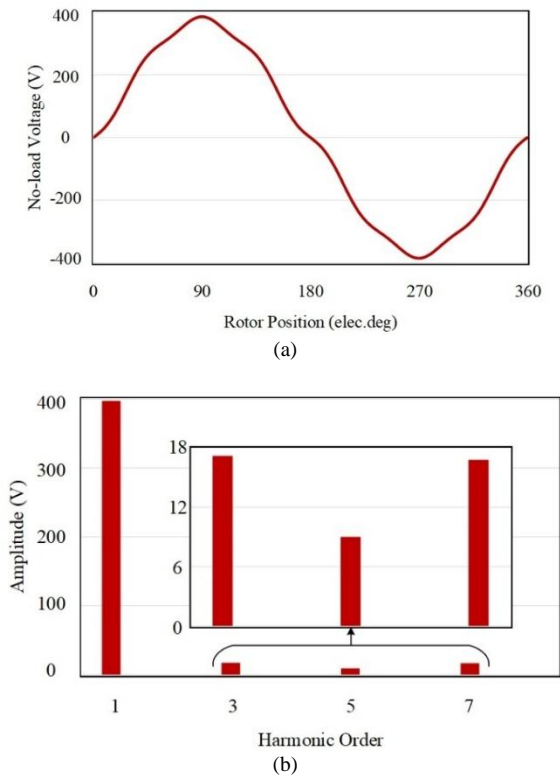
Proposed generator	No-load voltage (V)	THD%	Cogging Torque (N m)
Before optimization	315.26	11.2	0.98
After optimization	398.4	6.4	0.34

Furthermore, the shape of the waveform suggests the presence of harmonic content, which is further analyzed through the harmonic spectrum depicted in Fig. 5(b). The spectral analysis reveals a dominance of odd harmonics, with even harmonics being nearly negligible. This pattern is consistent with the inherent symmetry of the machine and confirms the proper alignment and magnetization of the PMs. The THD is computed to be approximately 6.4%, a level considered acceptable for many applications, especially considering the lack of filtering at this stage.

The relatively low THD also reflects the effectiveness of the structural and electromagnetic optimization strategies employed during the design phase.

Nevertheless, one of the main drawbacks associated with permanent magnet machines is the presence of cogging torque, an undesirable torque caused by the interaction between the permanent magnets and the stator's salient slots. This phenomenon is particularly pronounced at low rotational speeds, where the torque ripple can induce mechanical vibrations, acoustic noise, and potentially long-term degradation of the generator's components. As shown in Fig. 6(a), the cogging torque in the proposed design is well-controlled, with a peak amplitude of only 0.34 N m.

This reduction in cogging torque suggests that appropriate design techniques have been effectively implemented. Additionally, Fig. 6(b) presents the air-gap flux density distribution under no-load conditions. The waveform exhibits a peak flux density of approximately 1.3 T, occurring when the rotor teeth are aligned with the stator teeth.

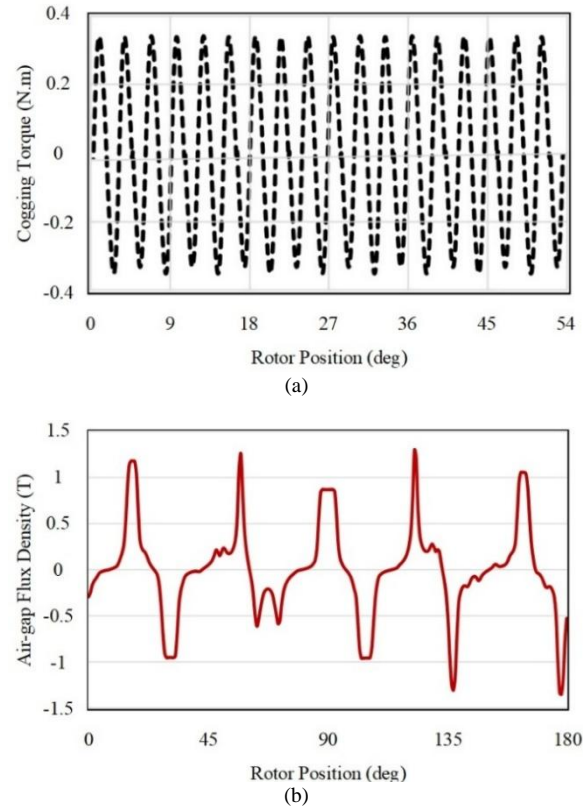


Figs. 5. The open-circuit phase voltage: (a) waveform; (b) harmonic spectrum

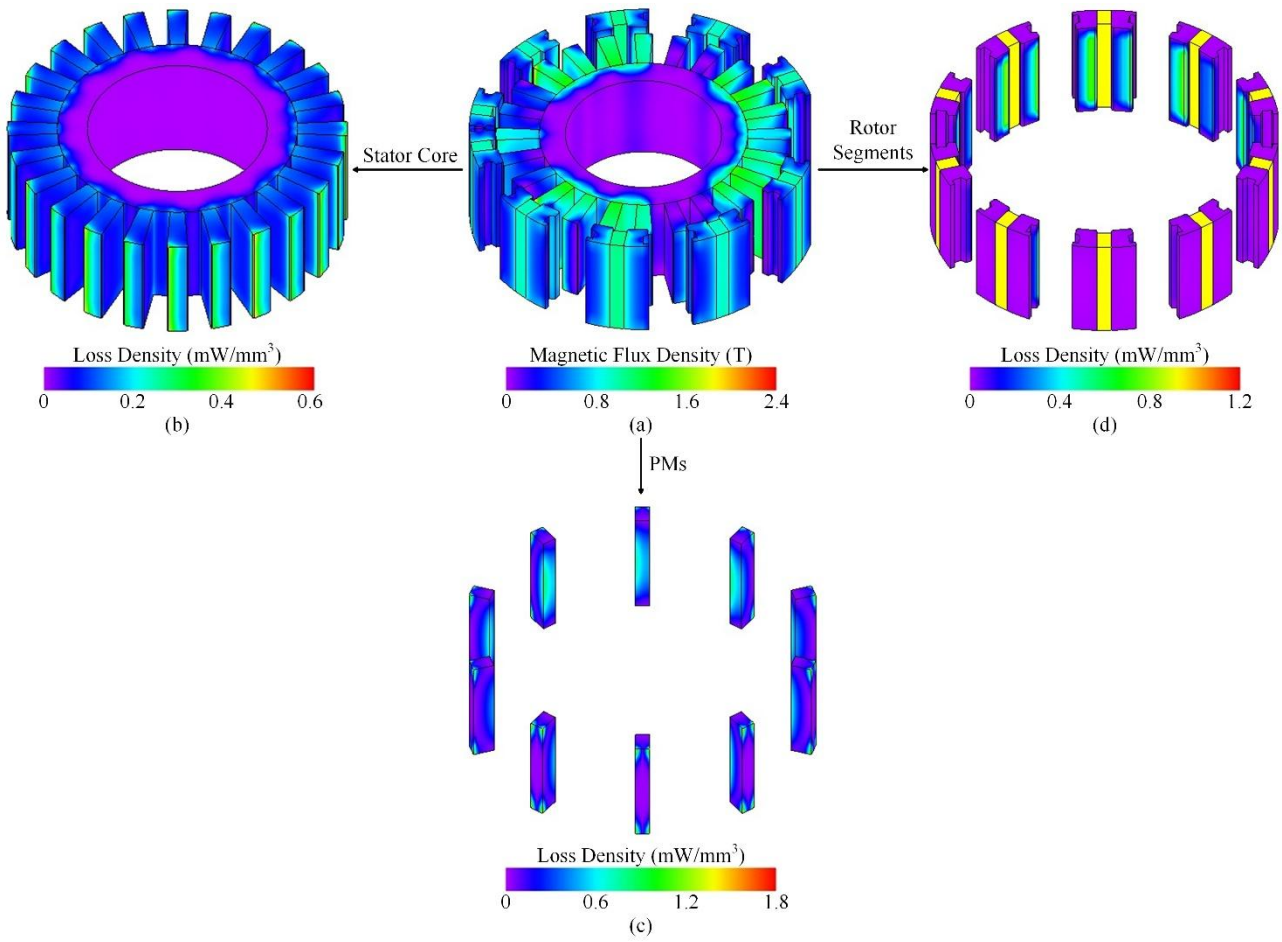
This alignment corresponds to the point of maximum magnetic coupling and signifies efficient utilization of the magnetic materials. The smooth profile of the flux waveform further supports the conclusion that the magnetic design is robust, with minimal flux leakage and saturation. Overall, these results demonstrate that the proposed generator not only meets performance expectations regarding voltage output and flux density but also effectively mitigates undesirable effects such as harmonics and cogging torque. The findings validate the proposed design approach and highlight its suitability for applications requiring stable and efficient power generation under varying load conditions.

IV.2. Full-load Characteristics

The rated-load condition provides a realistic operational scenario for assessing the generator's electromagnetic and thermal performance. Using a comprehensive 3D FEM analysis, the magnetic flux distribution, loss density profiles, and torque output have been thoroughly evaluated to ensure the design's robustness and efficiency. As illustrated in Fig. 7(a), the magnetic flux distribution within the generator under full-load operation reveals a well-balanced field pattern with no observable signs of magnetic saturation in either the stator or rotor components. The absence of saturation confirms that the core materials and geometric parameters have been effectively chosen to handle the magnetic loading at rated conditions.



Figs. 6. (a) Cogging torque waveform; (b) air-gap flux density at no-load condition



Figs. 7. (a) full-load magnetic flux density distribution; (b) loss density distribution in the stator core; (c) loss density distribution in the magnets; (d) loss density distribution in the rotor segments

A closer inspection reveals that the magnetic flux density within the stator teeth is notably higher than that in the stator yoke, which aligns with the expected magnetic path configuration. The teeth are the primary channel for magnetic flux linkage with the rotor, justifying their higher flux density levels. Losses within the machine are critical, not only because they reduce efficiency but also due to their thermal implications. Fig. 7(b) illustrates the core loss density across the stator, highlighting a pronounced loss concentration at the tooth-tips adjacent to the air gap. This localized increase can be attributed to the higher flux variation and field intensity experienced in these regions due to the proximity of the rotating magnets.

The elevated flux gradients in this interface zone intensify both hysteresis and eddy current losses, thereby necessitating careful thermal management strategies in these areas. Further detailed in Figs. 7(c) and 7 (d), the loss density distribution in the magnets and rotor segments shows an asymmetrical pattern. The surfaces of these components facing the air gap exhibit significantly higher loss densities than their inner regions. This trend can be directly linked to the dynamic interaction between the rotating magnetic field and the stator slots, which induces localized eddy currents and potential temperature rises.

Such findings underscore the importance of material

selection, especially for the magnets, where high electrical resistivity and temperature tolerance are desirable traits to mitigate performance degradation over time. The electromagnetic torque behavior, shown in Fig. 8, provides additional confirmation of the generator's operational stability under rated conditions. The average torque produced is approximately -33 N m, closely matching the design specifications. The torque waveform exhibits a ripple of around 6%, a value within acceptable bounds for many practical applications.

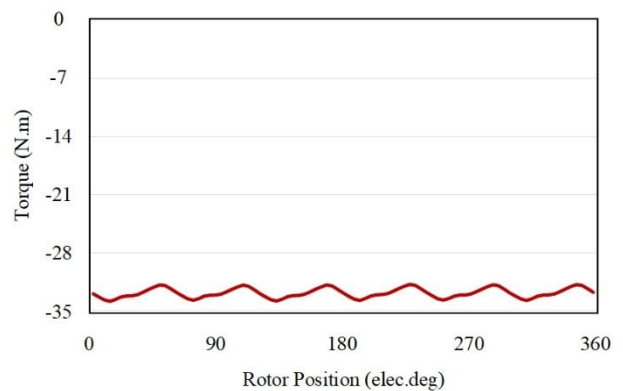
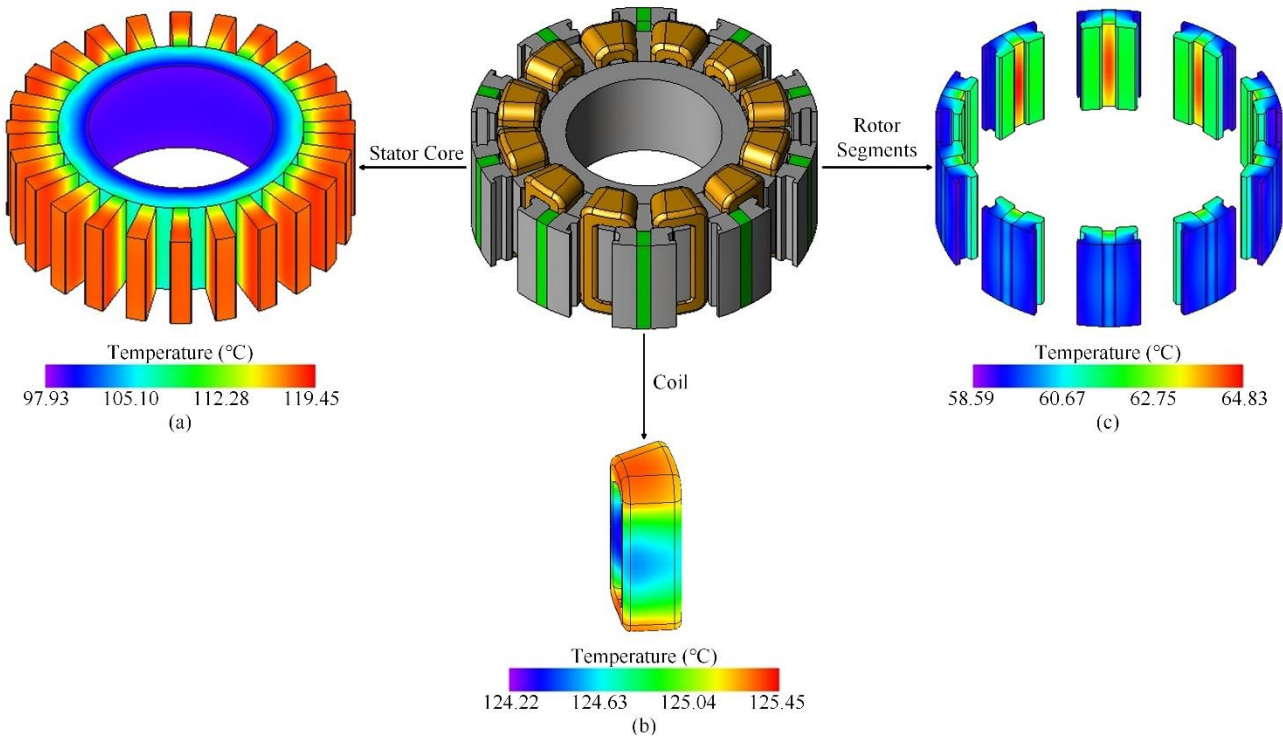


Fig. 8. Steady-state electromagnetic torque at rated load



Figs. 9. Temperature distribution: (a) stator core; (b) coil; (c) rotor segments and PMs

While some ripple is inevitable due to slotting effects and cogging influences, the relatively smooth torque profile demonstrates that the machine benefits from effective electromagnetic balancing and rotor-stator alignment. Minimizing torque ripple is crucial in applications where mechanical vibration, noise, or fatigue can adversely impact system reliability. Collectively, these results affirm the structural and electromagnetic integrity of the generator under full-load conditions. The balanced flux distribution, controlled loss concentration, and steady torque production highlight the efficacy of the design and its readiness for integration into real-world energy systems, especially where high efficiency and thermal reliability are paramount.

V. Thermal Analysis

After calculating the various losses that act as heat sources in the proposed generator through 3-D FEM analysis, a thermal analysis can be undertaken [45]. To accurately assess the thermal performance of the generator, it is crucial to calculate the thermal characteristics, particularly the heat transfer coefficients.

Since the generator is modeled using JMAG software, obtaining precise values for these coefficients is essential to minimize output errors. The coefficients can be categorized into three types: radiation, convection, and conduction. Their definitions and related equations are provided in [19].

V.1. Temperature Distribution

The temperature distribution within the proposed

generator, as presented in Figs. 9, offers significant insights into the thermal behavior of the stator and rotor components. In the steady-state thermal analysis of the stator core (Fig. 9(a)), it is evident that the highest temperature is concentrated at the stator teeth-tip, a region traditionally subject to higher magnetic flux densities and, consequently, more significant losses. This localized temperature rise aligns with expectations based on the typical distribution of electromagnetic losses within the stator core. The lowest temperature observed at the stator yoke is also consistent with thermal models, where less magnetic activity typically results in lower thermal stress.

The temperature differential of approximately 21.5 °C between the hottest (~119.5 °C) and coolest (~98 °C) points on the stator core is noteworthy. This gradient emphasizes the importance of thermal management, as such temperature variations may induce thermal stresses that could impact the longevity and operational stability of the generator. Given this, further investigation into advanced cooling techniques, such as fluid or air cooling, could be crucial for mitigating such gradients and ensuring uniform temperature distribution across the stator core.

Turning to the coil's temperature distribution, depicted in Fig. 9(b), the hottest spot is at the end-winding, registering a temperature of approximately 125.5 °C. The end-winding is a thermally critical region due to the concentration of electrical currents and the geometric configuration that impedes efficient heat dissipation. This observation confirms the need for specialized cooling strategies in the end-winding area to prevent overheating, which could lead to insulation degradation and a potential reduction in overall machine efficiency. In Fig. 9(c), the temperature distribution of the rotor segments and

magnets is shown. The sides of the rotor segments and magnets that face the air gap exhibit higher temperatures than those facing the rotor core, which can be attributed to the proximity of the air gap to the cooling medium. This temperature difference is significant as it highlights the importance of effective cooling mechanisms for the rotor, particularly the magnets, which are critical for the generator's performance. The average operating temperature of the magnets is approximately 63.5 °C, which is well below the threshold for neodymium magnets, typically around 80 °C, where demagnetization risks become prominent. This observation suggests that the risk of demagnetization is minimal, further supporting the thermal efficiency of the proposed generator design.

Despite the promising results, the thermal behavior observed in this analysis indicates potential areas for optimization. While the temperature distribution appears generally acceptable, localized hotspots, especially in the end-winding and stator teeth-tip regions, suggest opportunities for further refinement. Advanced cooling techniques, such as integrated cooling channels or heat sinks in the end-winding and stator core, could reduce temperature gradients and enhance the overall thermal management strategy. Moreover, incorporating thermal simulations under varying operational conditions (e.g., load cycles and ambient temperatures) could provide a more comprehensive understanding of the generator's long-term thermal stability and performance. In conclusion, the thermal analysis reveals that the proposed generator operates within acceptable temperature limits.

V.2. Temperature Rise

The transient-state temperatures of various generator components are illustrated in Fig. 10. The initial ambient temperature is 20 °C, and the simulation duration is 5 hours. It can be seen that after ~120 minutes, the transient state changes to the steady state. It is evident that the hottest spot in the generator is the winding, which reached a temperature of approximately 125 °C. Additionally, the average temperature of the stator core increased to about 110 °C.

The rotational components, such as the rotor segments and the magnets, exhibited nearly identical temperature readings. The rotor temperature reached around 61.5 °C, while the PM temperature increased to 63 °C. It is clear that the temperatures of stationary components are nearly double those of the rotating components. This disparity explains why neodymium magnets are installed in the rotor core, as these magnets are susceptible to demagnetization at high temperatures.

Finally, the other specifications of the generator are listed in Table IX. The rated output torque is 2243 W, the power density is 0.93 (W/cm³), and the efficiency of the generator is 86.5%. Additionally, the volume of the magnets is approximately 67.2 cm³, while the combined volume of the rotor and stator core is around 2356 cm³.

This indicates that the ratio of the magnets' volume to the total machine volume is 2.85%, indicating that the use of magnets is optimized.

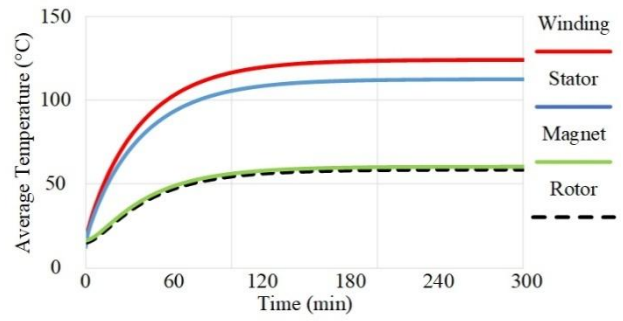


Fig. 10. Transient-state temperature of various components

TABLE IX
GENERATOR SPECIFICATIONS

Parameter	Value	Unit
Volume of the PMs	67.2	cm ³
Volume of the stator core	615.6	cm ³
Volume of the rotor core	1740.65	cm ³
Copper loss	238	W
Stator loss	38.66	W
Rotor loss	53.83	W
PMs loss	18.73	W
Output power	2243	W
Power density	0.93	W/cm ³
Efficiency	86.5	%
Ratio of PMs volume to total machine volume	2.85	%

In comparison, [20] shows a ratio of about 4.5% while achieving a slightly higher power density than the proposed generator in this paper. Furthermore, the stator core in the mentioned reference is considerably more complex, making the proposed generator a more cost-effective option.

VI. Discussion

The design and optimization of the outer rotor flux-switching permanent magnet generator presented in this study have demonstrated promising results, particularly concerning key performance parameters such as no-load voltage, THD, and cogging torque. Applying the Taguchi method-driven optimization process resulted in a remarkable 26% increase in no-load voltage, a significant 43% reduction in THD, and an impressive 65% decrease in cogging torque. These substantial improvements indicate the effectiveness of the chosen design parameters, confirming that the generator's performance has been enhanced in these critical areas compared to previous designs. In comparison, [19] achieves a slightly higher power density, around 4.5%, but this comes at the cost of a more complex stator core, which will likely increase production and operational costs. The simplicity and cost-effectiveness of the proposed design, coupled with its optimization results, position it as a highly competitive option in the field, offering a good balance between performance and manufacturability. The full-load electromagnetic analysis conducted on the proposed generator shows that the design is well-optimized for handling the expected magnetic loading at rated conditions. No signs of magnetic saturation were

observed, indicating that the generator's magnetic circuit is effectively balanced, preventing any degradation in performance. Furthermore, the torque profile exhibits minimal ripple and is well within acceptable limits, ensuring smooth and consistent operation even under variable load conditions. These findings suggest that the generator can operate efficiently in real-world applications, where stability and reliability are crucial.

Unlike some designs that may suffer from significant torque fluctuations, the minimal ripple in this generator's torque profile makes it an excellent candidate for systems requiring steady performance, such as wind turbines and other renewable energy applications. In addition to its electromagnetic characteristics, the generator's thermal performance is another area where the design has been optimized. Thermal analysis of the generator revealed a well-balanced temperature distribution across its components, ensuring that the generator remains thermally stable under full-load operation. While the stator and end-winding regions experience elevated temperatures due to localized electrical losses, these temperatures stay within safe operational limits, suggesting that the generator's thermal management system functions as intended. This effective heat dissipation is crucial for maintaining the generator's efficiency and longevity, preventing overheating that could lead to performance degradation or failure. The rotor components, particularly the neodymium magnets, remained well below their critical temperature, ensuring that the risk of demagnetization remained minimal throughout the generator's operation. This result underscores the careful design of the rotor system. It supports the decision to position the magnets within the rotor core rather than in the stator, as this placement reduces the overall thermal load on the magnets, further protecting their integrity. Compared to [19], which uses a similar magnet-to-volume ratio of 4.5%, the proposed design achieves a more optimized magnet-volume ratio of 2.85%. This lower magnet-to-volume ratio allows for a more efficient use of materials, significantly reducing the dependency on rare-earth magnets and thus lowering the cost of production. The reduced magnet volume also contributes to the overall efficiency of the generator, as it allows for a lighter and more compact design while still maintaining the required electromagnetic performance.

This aspect is crucial for applications such as wind turbines, where the efficient use of materials can lead to cost savings and improved sustainability. The generator's thermal management is also an essential consideration in its design, and the results show that the generator is able to handle the heat generated during operation without the need for complex or excessive cooling systems. The temperature profile of the generator indicates that the stationary components, such as the stator and end windings, naturally experience higher temperatures due to the electrical losses associated with current flow.

However, these higher temperatures are well-distributed and do not reach levels that would affect the long-term performance or reliability of the machine. On

the other hand, the rotor, specifically the magnets, remains cooler, demonstrating the thermal design's effectiveness in maintaining the system's stability. In contrast to the design in [19], which addresses the higher power density with more intricate cooling solutions and a more complex core design, the proposed generator in this study shows that it can achieve similar performance with a more straightforward design that reduces cost and complexity.

This simplified design not only makes the generator more cost-effective but also enhances its reliability by minimizing the number of components that could fail or require maintenance. This is particularly advantageous for large-scale industrial applications, where downtime and maintenance costs are a significant concern. Overall, the proposed outer rotor flux-switching permanent magnet generator represents a substantial advancement in generator design. The optimization process has successfully enhanced both its electromagnetic performance and thermal stability. The generator's lower magnet-to-volume ratio and efficient thermal management system ensure that it can operate reliably and sustainably while keeping production costs lower compared to designs like [19]. By offering excellent performance with a more efficient use of materials and a more cost-effective design, the generator holds great promise for large-scale applications in renewable energy sectors, especially for wind power generation, where performance and material efficiency are crucial factors.

VII. Conclusion

This paper introduces a new outer rotor flux-switching permanent magnet generator specifically designed for wind turbine applications. It begins by outlining the key analytical equations related to the generator and then explains how the initial design was optimized using the Taguchi method. The primary goals of this optimization were to increase the no-load phase voltage and reduce the total harmonic distortion of the voltage and cogging torque. The optimization resulted in approximately a 26% increase in no-load voltage, a ~43% reduction in THD, and a ~65% decrease in cogging torque. Additionally, the full-load electromagnetic performance of the generator showed no signs of magnetic saturation, with an average output torque of around -33 N m. From a thermal evaluation standpoint, the temperature of the stationary components was nearly double that of the rotating components. This finding justifies the placement of neodymium magnets in the rotor core rather than the stator, as these magnets are prone to demagnetization under high-temperature conditions. Furthermore, the generator exhibited a power density of 0.93 (W/cm³). The magnets' ratio to the total machine volume was 2.85%.

This indicates that using neodymium magnets was optimal, confirming that this generator can be classified as a high-power density machine. Future research will optimize the housing and segment the PMs to mitigate losses and lower the generator's operating temperature while enhancing power density. Furthermore, the

subsequent publication will employ computational fluid dynamics to support this investigation.

References

- [1] T. Vasylieva, O. Lyulyov, Y. Bilan, and D. Streimikiene, Sustainable economic development and greenhouse gas emissions: The dynamic impact of renewable energy consumption, GDP, and corruption, *Energies*, vol. 12, no. 17, p. 3289, 2019.
- [2] A. Qazi et al., Towards sustainable energy: a systematic review of renewable energy sources, technologies, and public opinions, *IEEE Access*, vol. 7, pp. 63837-63851, 2019.
- [3] N. Maamoun, R. Kennedy, X. Jin, and J. Urpelainen, Identifying coal-fired power plants for early retirement, *Renewable and Sustainable Energy Reviews*, vol. 126, p. 109833, 2020.
- [4] M. S. Alam, F. S. Al-Ismaïl, A. Salem, and M. A. Abido, High-level penetration of renewable energy sources into grid utility: Challenges and solutions, *IEEE Access*, vol. 8, pp. 190277-190299, 2020.
- [5] E. T. Sayed et al., Renewable energy and energy storage systems, *Energies*, vol. 16, no. 3, p. 1415, 2023.
- [6] T.-Z. Ang, M. Salem, M. Kamarol, H. S. Das, M. A. Nazari, and N. Prabaharan, A comprehensive study of renewable energy sources: Classifications, challenges and suggestions, *Energy Strategy Reviews*, vol. 43, p. 100939, 2022.
- [7] G. J. Herbert, S. Iniyar, E. Sreevalsan, and S. Rajapandian, A review of wind energy technologies, *Renewable and sustainable energy Reviews*, vol. 11, no. 6, pp. 1117-1145, 2007.
- [8] P. Tchakoua, R. Wamkeue, M. Ouhrouche, F. Slaoui-Hasnaoui, T. A. Tameghe, and G. Ekemb, Wind turbine condition monitoring: State-of-the-art review, new trends, and future challenges, *Energies*, vol. 7, no. 4, pp. 2595-2630, 2014.
- [9] W. Li and M. Cheng, Reliability analysis and evaluation for flux-switching permanent magnet machine, *IEEE Transactions on Industrial Electronics*, vol. 66, no. 3, pp. 1760-1769, 2018.
- [10] P. Seangwong, S. Chamchuen, N. Fernando, A. Siritaratiwat, and P. Khunkitti, A Novel Six-Phase V-Shaped Flux-Switching Permanent Magnet Generator for Wind Power Generation, *Energies*, vol. 15, no. 24, p. 9608, 2022.
- [11] C. Nissayan, P. Seangwong, S. Chamchuen, N. Fernando, A. Siritaratiwat, and P. Khunkitti, Modeling and optimal configuration design of flux-barrier for torque improvement of rotor flux switching permanent magnet machine, *Energies*, vol. 15, no. 22, p. 8429, 2022.
- [12] M. G. Neto, F. F. da Silva, and P. J. d. C. Branco, Operational Analysis of an Axial and Solid Double-Pole Configuration in a Permanent Magnet Flux-Switching Generator, *Energies*, vol. 17, no. 7, p. 1698, 2024.
- [13] A. Zarghani, M. Farahzadi, A. Ghaheri, and K. Abbaszadeh, Accurate 3D Thermal Network Development for Direct-drive Outer-rotor Hybrid-PM Flux-switching Generator, *Chinese Journal of Electrical Engineering*, vol. 10, no. 2, pp. 80-92, 2024.
- [14] V. I. Vlachou et al., Overview on Permanent Magnet Motor Trends and Developments, *Energies*, vol. 17, no. 2, p. 538, 2024.
- [15] M. Azeem and B. Kim, Electromagnetic analysis and performance investigation of a flux-switching permanent magnet machine, *Energies*, vol. 12, no. 17, p. 3362, 2019.
- [16] G. Zhang, Q. Tong, A. Qiu, X. Xu, W. Hua, and Z. Chen, Parameter Sensitivity Analysis and Robust Design Approach for Flux-Switching Permanent Magnet Machines, *Energies*, vol. 15, no. 6, p. 2194, 2022.
- [17] J. Cao, X. Guo, W. Fu, R. Wang, Y. Liu, and L. Lin, A method to improve torque density in a flux-switching permanent magnet machine, *Energies*, vol. 13, no. 20, p. 5308, 2020.
- [18] J. Zhao, Y. Zheng, C. Zhu, X. Liu, and B. Li, A novel modular-stator outer-rotor flux-switching permanent-magnet motor, *Energies*, vol. 10, no. 7, p. 937, 2017.
- [19] M. Farahzadi, K. Abbaszadeh, and S. Mirmikjoo, Electromagnetic-thermal analysis of a hybrid-excited flux switching permanent magnet generator for wind turbine application, *IEEE Transactions on Energy Conversion*, vol. 38, no. 3, pp. 1962-1973, 2023.
- [20] S. M. Saghin, A. Ghaheri, H. Shirzad, and E. Afjei, Performance optimisation of a segmented outer rotor flux switching permanent magnet motor for direct drive washing machine application, *IET Electric Power Applications*, vol. 15, no. 12, pp. 1574-1587, 2021.
- [21] J. Zhao, W. Fu, Y. Zheng, Z. Chen, and Y. Wang, Comparative study of modular-stator and conventional outer-rotor flux-switching permanent-magnet motors, *IEEE Access*, vol. 7, pp. 38297-38305, 2019.
- [22] B. Ullah, F. Khan, Z. Ahmad, S. Akbar, A. H. Milyani, and A. A. Azhari, Performance analysis of a modular E-shaped stator hybrid excited flux switching motor with flux gaps, *IEEE Access*, vol. 10, pp. 116098-116106, 2022.
- [23] Z. Chen and Y. Cui, Numerical simulation and experimental validation of a flux switching permanent magnet memory machine, *IEEE Access*, vol. 8, pp. 194904-194911, 2020.
- [24] W. Ullah, F. Khan, E. Sulaiman, M. Umair, N. Ullah, and B. Khan, Analytical validation of novel consequent pole E-core stator permanent magnet flux switching machine, *IET Electric Power Applications*, vol. 14, no. 5, pp. 789-796, 2020.
- [25] X. Cai, M. Cheng, S. Zhu, and J. Zhang, Thermal modeling of flux-switching permanent-magnet machines considering anisotropic conductivity and thermal contact resistance, *IEEE Transactions on Industrial Electronics*, vol. 63, no. 6, pp. 3355-3365, 2016.
- [26] M. Cheng, J. Wang, S. Zhu, and W. Wang, Loss calculation and thermal analysis for nine-phase flux switching permanent magnet machine, *IEEE Transactions on Energy Conversion*, vol. 33, no. 4, pp. 2133-2142, 2018.
- [27] D. Liang et al., Estimation of 3-D magnet temperature distribution based on lumped-parameter and analytical hybrid thermal model for SPMSM, *IEEE Transactions on Energy Conversion*, vol. 37, no. 1, pp. 515-525, 2021.
- [28] R. Burke, A. Giedymis, Z. Wu, H. Chuan, N. Bourne, and J. G. Hawley, A lumped parameter thermal model for single-sided AFPM machines with experimental validation, *IEEE Transactions on Transportation Electrification*, vol. 6, no. 3, pp. 1065-1083, 2020.
- [29] A. Glowacz, Thermographic fault diagnosis of ventilation in BLDC motors, *Sensors*, vol. 21, no. 21, p. 7245, 2021.
- [30] A. Glowacz, Fault diagnosis of electric impact drills using thermal imaging, *Measurement*, vol. 171, p. 108815, 2021.
- [31] A. Glowacz, Ventilation diagnosis of angle grinder using thermal imaging, *Sensors*, vol. 21, no. 8, p. 2853, 2021.
- [32] R. Nasiri-Zarandi, A. Ghaheri, and K. Abbaszadeh, Thermal modeling and analysis of a novel transverse flux HAPM generator for small-scale wind turbine application, *IEEE Transactions on Energy Conversion*, vol. 35, no. 1, pp. 445-453, 2019.
- [33] A. Zarghani, H. Torkaman, N. Arbab, and M. S. Toulabi, Lumped parameter thermal network for thermal analysis of a rotor-excited axial flux switching machine with electromagnetic-thermal design, *Measurement*, vol. 193, p. 110971, 2022.
- [34] R. Balat, A review of modern wind turbine technology, *Energy Sources, Part A*, vol. 31, no. 17, pp. 1561-1572, 2009.
- [35] A. Tummala, R. K. Velamati, D. K. Sinha, V. Indraj, and V. H. Krishna, A review on small scale wind turbines, *Renewable and Sustainable Energy Reviews*, vol. 56, pp. 1351-1371, 2016.
- [36] V. L. Okulov and G. A. Van Kuik, The Betz-Joukowski limit: on the contribution to rotor aerodynamics by the British, German and Russian scientific schools, *Wind Energy*, vol. 15, no. 2, pp. 335-344, 2012.
- [37] J. D. De Koning, L. Gevaert, J. Van de Vyver, T. L. Vandoorn, and L. Vandeveldel, Online estimation of the power coefficient versus tip-speed ratio curve of wind turbines, in *IECON 2013-39th Annual Conference of the IEEE Industrial Electronics Society*, 2013: IEEE, pp. 1792-1797.
- [38] Tammaruckwattana, S., Reangkittakarn, S., Suppaadirek, N., Ohyama, K., Experimental Verification of Wind Power Generation System Using Diode Bridge Rectifier Circuit with Wind Turbine Simulator, (2022) *International Review of Electrical Engineering (IREE)*, 17 (1), pp. 54-65.
doi: <https://doi.org/10.15866/iree.v17i1.20524>
- [39] W. Tong, *Wind power generation and wind turbine design*. WIT press, 2010.
- [40] Y. Shi, L. Jian, J. Wei, Z. Shao, W. Li, and C. C. Chan, A new perspective on the operating principle of flux-switching permanent-magnet machines, *IEEE Transactions on Industrial Electronics*, vol. 63, no. 3, pp. 1425-1437, 2015.

- [41] W. Ullah, F. Khan, and S. Hussain, A comparative study of dual stator with novel dual rotor permanent magnet flux switching generator for counter rotating wind turbine applications, *IEEE Access*, vol. 10, pp. 8243-8261, 2022.
- [42] W. Hua, H. Zhang, M. Cheng, J. Meng, and C. Hou, An outer-rotor flux-switching permanent-magnet-machine with wedge-shaped magnets for in-wheel light traction, *IEEE Transactions on Industrial Electronics*, vol. 64, no. 1, pp. 69-80, 2016.
- [43] C. Qu, Z. Guo, Y. Hu, X. Wang, and F. Han, Multi-objective optimization design of a new permanent magnet synchronous motor based on the taguchi Method, *Energies*, vol. 15, no. 19, p. 7347, 2022.
- [44] F. Mahmouditabar and N. J. Baker, Design Optimization of Induction Motors with Different Stator Slot Rotor Bar Combinations Considering Drive Cycle, *Energies*, vol. 17, no. 1, p. 154, 2023.
- [45] Vijayasree, G., Mini, V., Ushakumari, S., Electrical Analysis of High-Speed Homopolar Inductor Alternator Using FEM, (2024) *International Review of Aerospace Engineering (IREASE)*, 17 (4), pp. 142-151.
doi:<https://doi.org/10.15866/irease.v17i4.25385>

Authors' information

¹Faculty of Electrical Engineering, K. N. Toosi University of Technology, Tehran 16317-14191, Iran.

²Faculty of Electrical Engineering, University of Science and Culture, Tehran 14619-68151, Iran.

³Electrical Engineering Department, Tampere University, 33100 Tampere, Finland.

⁴Faculty of Electrical Engineering, Shahid Beheshti University, Tehran 19839-69411, Iran.

⁵Faculty of Electrical and Information Engineering, University of Cassino and Southern Lazio, 03043 Cassino, Italy



Amir Ebrahimi Shohani was born in Qom, Iran, in 1996. He received his B.Sc. in Electrical Engineering from Sahand University of Technology in Tabriz, Iran, in 2018, and his M.Sc. in Electric Machines and Power Electronics from K. N. Toosi University of Technology in Tehran, Iran, in 2021. He has over a year and a half of work experience and has served as both a teaching assistant and a research assistant. His research interests include designing and analyzing electric machines, particularly flux-switching machines, vernier machines, axial flux machines, and permanent magnet synchronous machines.



Mohammad Farahzadi was born in Tehran, Iran, in 1992. He received his M.Sc. degree in Power Electronics and Electric Machines in 2021. He is currently an Electrical Machine Designer with the Niroo Research Institute, Tehran, Iran, and a Researcher with the laboratory, K. N. Toosi University of Technology, Tehran, Iran. He is among the top researchers internationally in thermal analysis employing 3-D FEM, CFD, and 3-D LPTN for various types of electric machines. He has authored papers in Q1 journals, such as *IEEE Transactions on Energy Conversion*, *IEEE Transactions on Transportation Electrification*, *IEEE Access*, and the *Chinese Journal of Electrical Engineering*. His research interests include mechanical and electromagnetic analyses by FEM (2D/3D), assessment of demagnetization of permanent magnets, thermal modeling by FEM, LPM, and CFD, and design, optimization, and prototyping of electric machines, especially machines of the flux switching permanent magnet, permanent magnet-assisted synchronous reluctance, radial flux permanent magnet, axial flux permanent magnet, and doubly salient permanent magnet.



Sohrab Abbasian (Student Member, IEEE) was born in Babol, Iran, in 1995. He received the B.Sc. degree from Babol Noshirvani University of Technology, Babol, in 2018, and the M.Sc. degree in electrical power engineering and power electronics from the K. N. Toosi University of Technology, Tehran, Iran, in 2021. He is currently pursuing his Ph.D. degree in power electronics engineering at Tampere University. His research interests include ac-dc, dc-dc power converters, high gain dc-dc converters, soft-switching techniques for dc-dc converters, and renewable energy conversion.



Aghil Ghaheri received his M.Sc. degree in Power Electronics and Electrical Machinery in 2016 and his Ph.D. degree in Electrical Machinery in 2022, both from Shahid Beheshti University in Tehran, Iran. From 2022 to 2024, he worked as a postdoctoral researcher in the Department of Electrical Engineering at Shahid Beheshti University. In 2024, he became an Assistant Professor in the same Department. His research interests include electromagnetic, thermal, and structural modeling, as well as the optimization and manufacturing of electric machines for industrial and renewable energy applications.



Karim Abbaszadeh (Senior Member, IEEE) received the B.S. degree in communication engineering from the Khaled Nasir Toosi University of Technology, Tehran, Iran, in 1991, and the M.S. and Ph.D. degrees in electrical engineering from the Amir Kabir University of Technology, Tehran, in 1997 and 2000, respectively. From 2001 to 2003, he was a Research Assistant with the Department of Electrical Engineering, Texas A&M University, College Station, TX, USA. He is currently a Professor at the Department of Electrical Engineering, K. N. Toosi University of Technology. He is actively involved in presenting short courses and consulting in his area of expertise in various industries. He is the author of more than 50 published journal articles. His research interests include power electronics and DC-DC and DC-AC converters, electric machinery, variable-speed drives, and propulsion applications.



Salman Ali (Graduate Student Member, IEEE) is a doctoral research student at the Università degli Studi di Cassino e del Lazio Meridionale, Italy. Ali received his BS in Electrical Engineering from Federal Urdu University Islamabad and his Masters in Electrical Engineering from COMSATS University Islamabad. His field of research is electrical engineering, specializing in electrical machine design. He is well-versed in power electronics, renewable energy technologies, and power and energy. Salman Ali is currently the Secretary of the Industrial Electronics Chapter of the IEEE Italy Section. As a young researcher, Salman has fourteen publications, including a patent.